Appendix to "Eph-ephrin signaling modulated by polymerization and condensation of receptors"

SI FIGURES AND LEGENDS

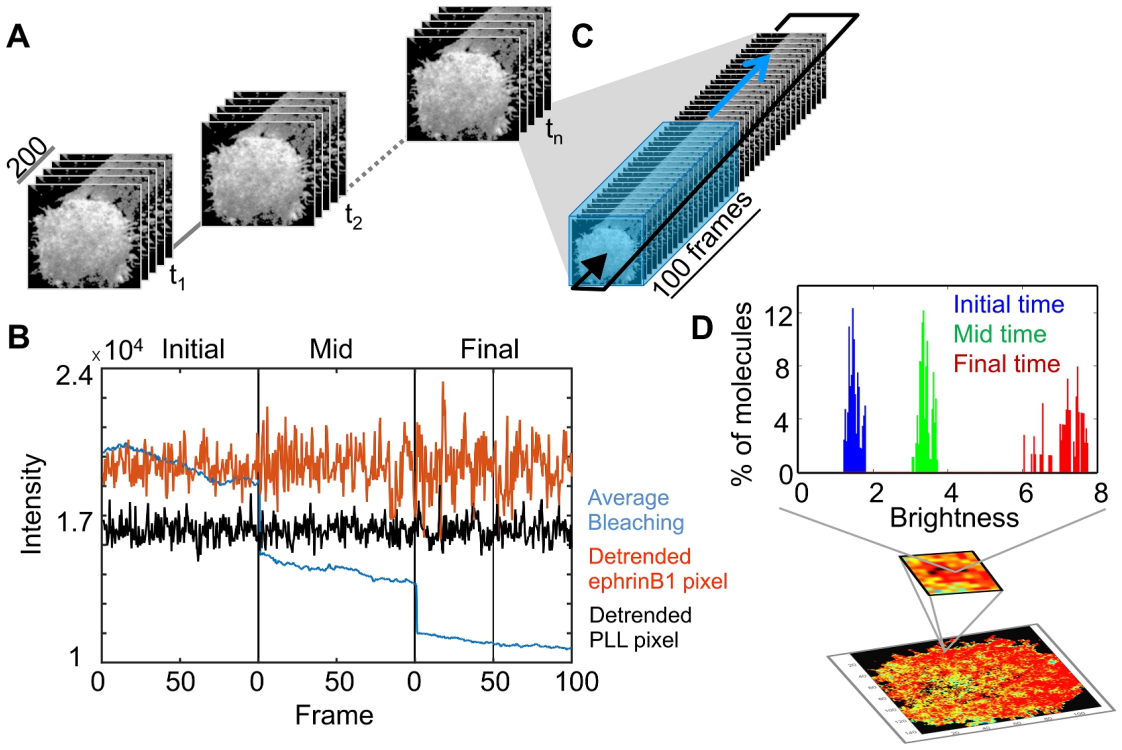

Figure S1: Enhanced Number and Brightness (eN&B). (a) N&B protocol extended over n time points. For every time point a batch of 200 images was acquired at 2Hz; subsequent time points were separated by $\tilde{5}$ minutes over a 60 minute period. (b) Fluorescence intensity fluctuations from single pixels at initial, mid and final experimental timepoint. The blue line depicts the fluorescence intensity averaged for an entire cell. The red and black lines depict the signal from single pixels from cells presented with ephrinB1 or PLL, respectively, after photobleaching compensation 24,25 (see Methods).(c) Oligomeric distribution in each pixel was achieved by statistically resampling 100 images out of the complete 200-image; the apparent number of molecules (N) and the brightness values (B) was calculated for each pixel in the image. This was repeated 200 times, for 100 image sub-samples starting with each of the 200 images (for statistical resampling, the set is "circularized" by moving the sliding window from image 200 to image 1). (d) Enhanced pixel brightness distributions. The analysis generates a matrix $M_{ij}(t)$ containing the distribution of brightness species for every (i,j) pixel in the cell ROI for every time point t. The histogram shows the brightness distributions of a single pixel at three different time points.

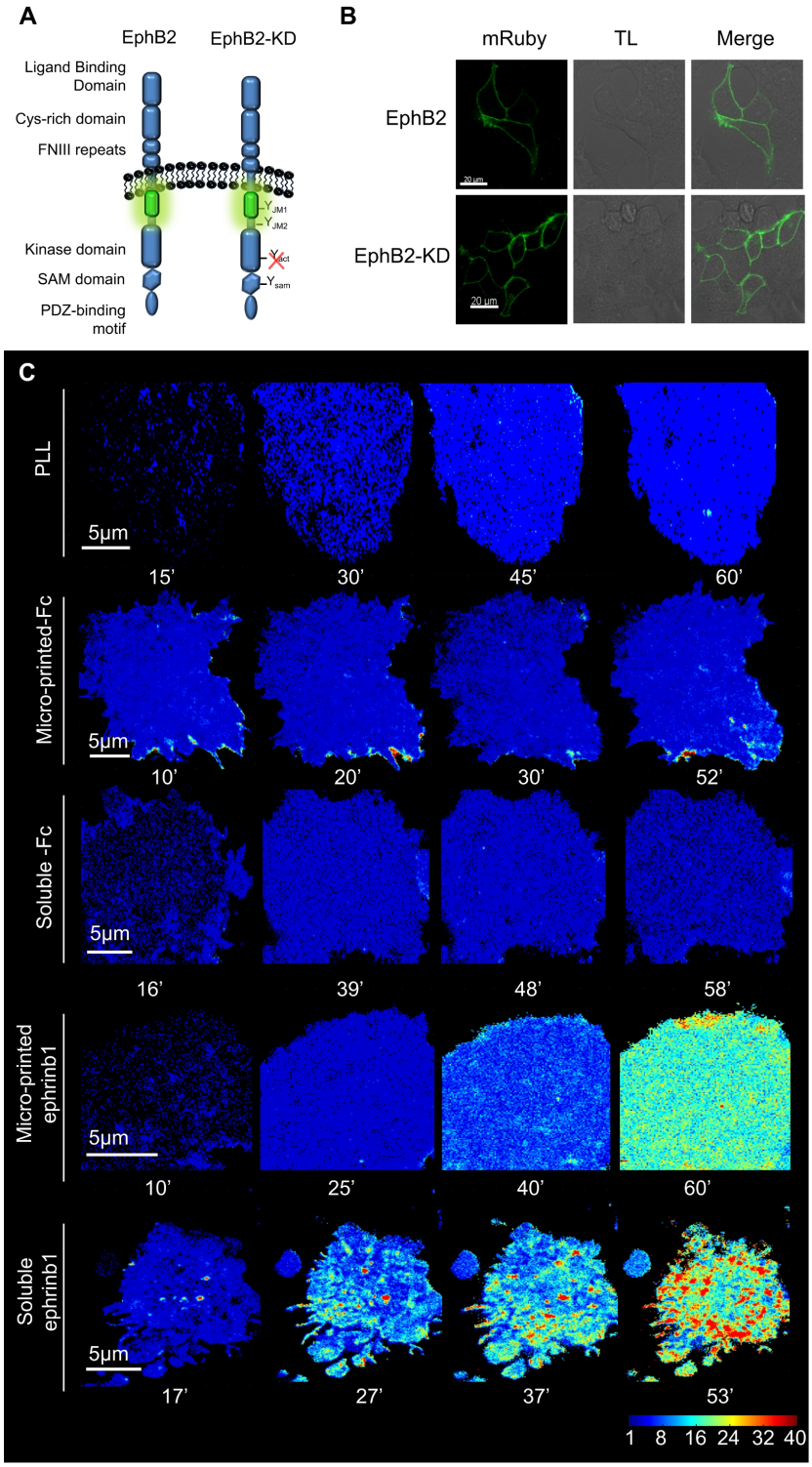
A
EphB2
EphB2-KD
Ligand Binding Domain
Cys-rich domain
FNIII repeats
Kinase domain
SAM domain
PDZ-binding motif
B
mRuby
TL
Merge
EphB2
EphB2-KD
20 µm
C
PLL
Micro-printed-Fc
Soluble -Fc
Micro-printed ephrinb1
Soluble ephrinb1
5µm
15'
30'
45'
60'
10'
20'
52'
16'
39'
48'
58'
25'
40'
17'
27'
37'
53'
1 8 16 24 32 40
D
micro-printed ephrinB1
soluble ephrinB1
micro-printed Fc
soluble Fc
% relative abundance
Oligomerization
E
A_i/R_0
Time (mins)

Figure S2: EphB2 Kinase Deficient (KD) mutant. (A) Schematic representation of the native EphB2 receptor and the KD mutant including a replacement Lys 660 to Arg as described (17, 18). (B) Fluorescent (mRuby) and transmitted light (TL) images of HEK293T cells transiently expressing EphB2_mruby or ephB2-KD_mRuby fusion proteins. Fig. 3. EphB2 Kinase Deficient (KD) mutant oligomerization. (C) Time-lapse brightness map of HEK293T:EphB2_KD cells acquired with the TIRF microscope. The cells were seeded on plates functionalized with 2μM Fc protein, 2μM ephrinB1 or presented with 0.2μM Fc or 0.2μM ephrinB1 in solution. Every pixel in the cell depicts the weighted average i-mer aggregate color-coded according to the color scale bar. (D) Distribution of average and standard deviation brightness values for multiple HEK293T:EphB2_KD cells (N¿5) that have been presented with the relevant ligand for 60 minutes. (E) i-mer evolution plot (see SI Materials and Methods). Evolution of the concentration of each aggregate (A_i) over time from the ephrinB1 stimulated cell in (C), normalized by the initial concentration of free receptor (R_0). i-mer values are color-coded according to the color scale bar.

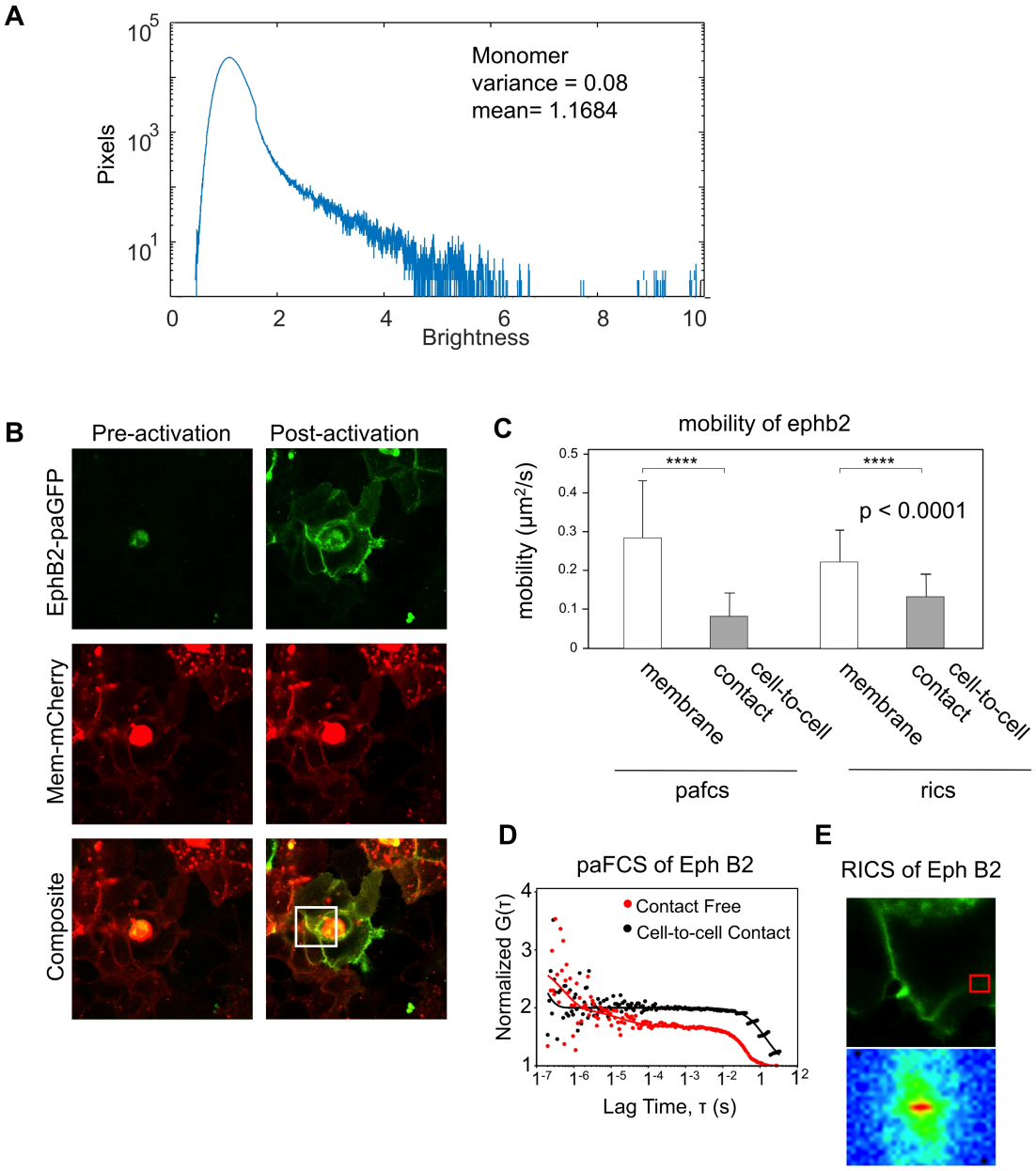

Figure S3: Monomer calibration. (a) Monomer brightness calibration. Brightness distribution combined for N=4 cells that have been plated on polylysine coated plates 48h with no additional treatment. Average brightness and variance are indicated. (b) EphB2-paGFP motility. Prior to photoactivation EphB2-paGFP is not fluorescent, however once activated, fluorescence signal was observed along the plasma membrane, colocalizing with the mem-mCherry as a point of reference. The photoactivation enables a subgroup of EphB2-paGFP present to be observed, thus providing more accurate FCS and RICS acquisition. (c) Analysis of the mobility of Eph B2-paGFP performed along membranes lacking cell-to-cell interactions using both paFCS and RICS. The mobility in contact-free membranes is 3-fold faster than when cell-to-cell contacts are present. (d) Autocorrelation function curves indicative of mobility at cell-to-cell contacts (red: 0.413 $\mu m^2/s$) and contact free membranes (black: 0.030 $\mu m^2/s$). (e) Example of RICS analysis.

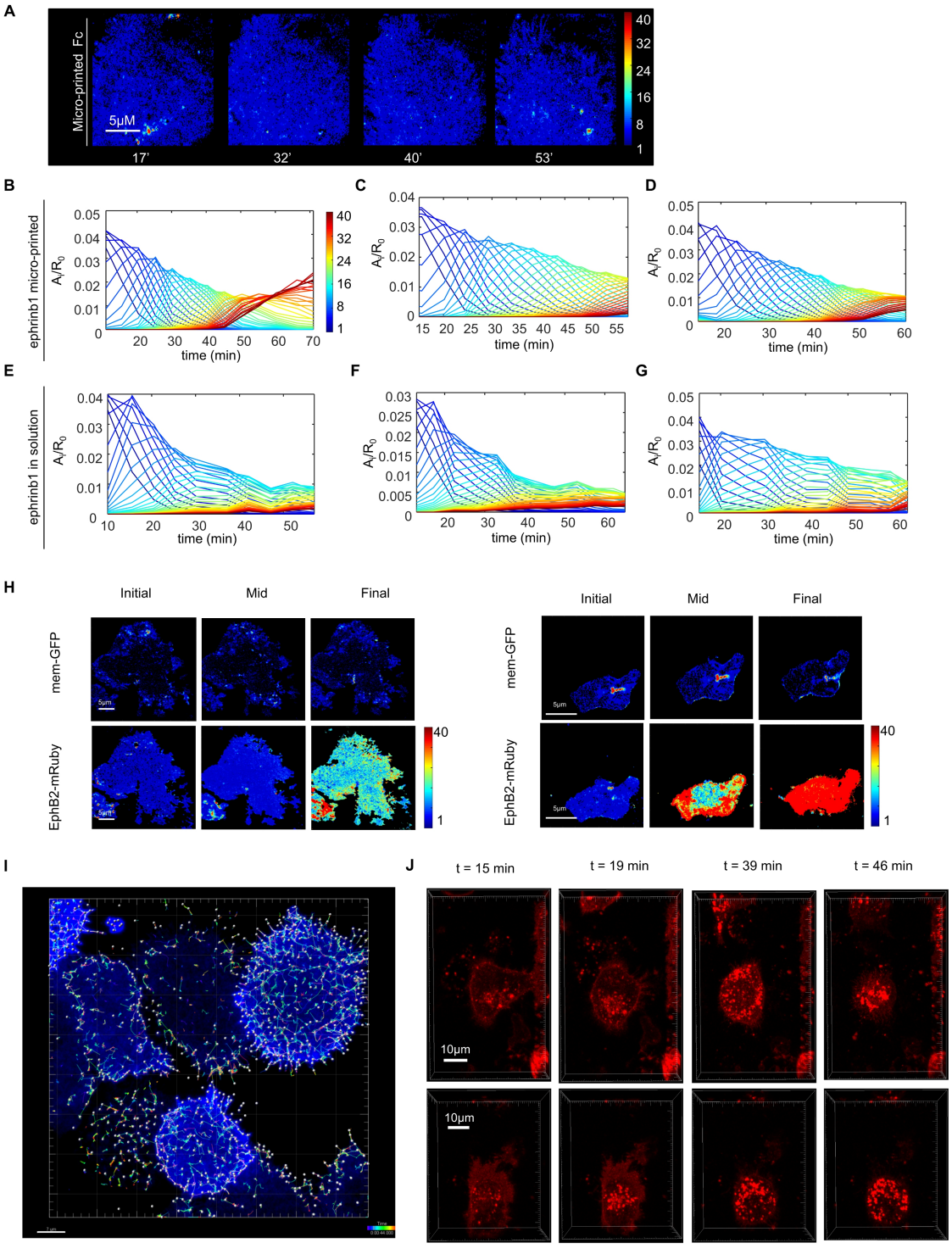

Figure S4: Additional eN&B analysis. i-mer plots show a reproducible clustering dynamics across cells and runs interrupted for at least 75 minutes. (a) eN&B brightness map of a HEK293T:EphB2_mRuby cell presented with 2μM micro-printed human Fc. The plots show the evolution of the concentration of each aggregate (A_i) over time from different ephrinB1-stimulated cells, normalized by the initial concentration of free receptor (R_0). The i-mer value of every curve is color-coded according to the color scale bar. (b-d) Three different instances corresponding to three independent cells stimulated with 2μM micro-printed ephrinB1. (e-g) Three different instances corresponding to independent cells stimulated with 0.2μM ephrinB1in solu-

tion. (h) Two instances of an EphB2-mRuby transgenic cell co-expressing membrane GFP (see methods). The cells were stimulated with 0.2μM ephrinB1in solution and eN&B analysis was performed in parallel in the green (GFP) and red (mRuby) channels. The initial point corresponds to images taken before stimulation. The mid and final point correspond to 30 and 60 min post stimulation, respectively.(i) Automated tracking of the 10% brighter clusters on cells after 45 min ephrin stimulation. The lines depict the trajectories of the clusters during the acquisition of 200 frames at 500ms frame rat (total of 100sec acquisition).(j) Snapshots of a time-lapse movie of HEK293T:EphB2_mRuby cells seeded onto surfaces micro-printed with ephrinB1. The images are maximum projections reconstructions of 3D confocal stacks.

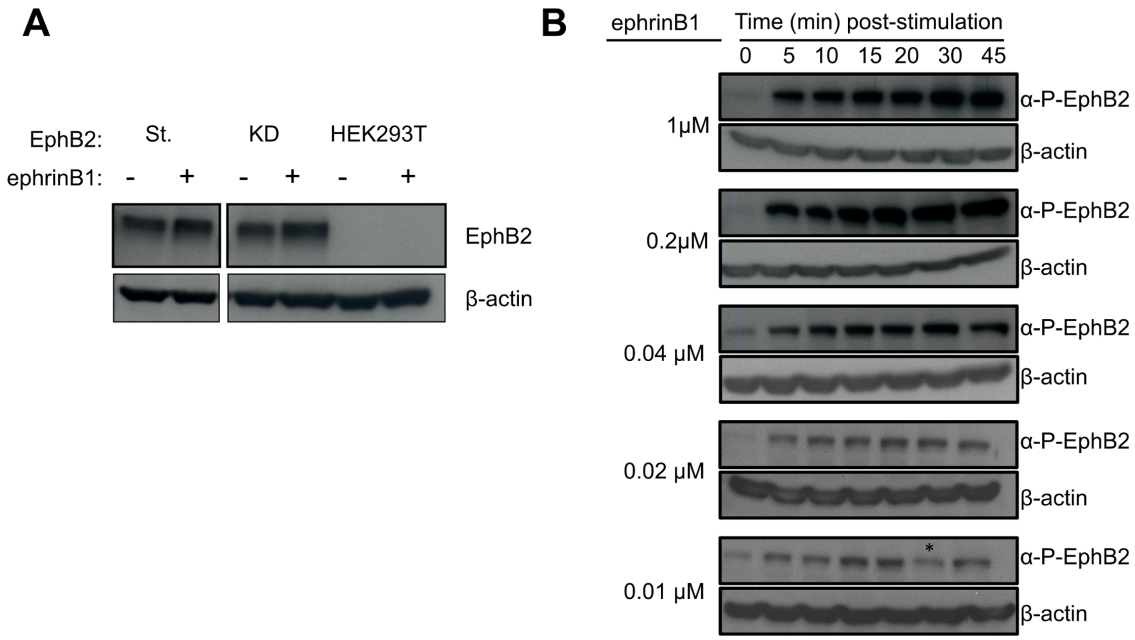

Figure S5: Endogenous EphB2 expression and phosphorylation kinetics. (a) Western Blot detection of total EphB2 (endogenous and transgenic) on HEK293T cells stably expressing the standard EphB2_mRuby receptor (St.), the kinase deficient (KD) mutant or the original (non-transduced) HEK293T cells, after 45 mins. of stimulation with or without 0.2 μM soluble ephrinB1. β-actin detection was used as a loading control. (b) EphrinB1 dose-dependent response of EphB2 phosphorylation. HEK293T cells stably expressing EphB2_mRuby were stimulated with the specified concentrations of ephrinB1. At the indicated times, the cells were harvested and lisated for protein extraction. All five time-courses were performed in parallel the same day to obtain a more precise comparison between kinetics. Western Blot detection was done using a specific phospho-antibody that recognized the phosphorylated fraction of the EphB2 receptor. β-actin was also detected as a loading control.* Time point removed from the analysis due to incomplete sample loading.

SI MATERIALS AND METHODS

Surface Coating and soluble ligand preparation

35 mm Glass bottom dishes (MatTek) were coated with poly-L-lysine (Sigma-Aldrich) solution at 0.05% (w/v) in PBS for 90 min and then rinsed with PBS and Milli-Q water. Flat Polydimethylsiloxane (PDMS) stamps (SYLGARD® 184 , Ellsworth Adhesives) were fabricated by mixing a 10:1 mass ratio of silicon elastomer base and curing agent. PDMS was degassed under vacuum, poured on flat Petri dishes and cured overnight at 60ºC. Stamps were cut in 12 mm round discs and cleaned with ethanol in an ultrasonic bath for 5 min. 2 μM recombinant mouse ephrinB-Fc Chimera or Recombinant Human IgG_1 Fc (R&D Systems Inc.) solution, hereafter referred as Fc, were conjugated with Goat Anti-Human IgG (Jackson ImmunoResearch 109-005-088) at a 2:5 molar ratio for 30 min under constant shaking. Thereafter, stamps were inked with ephrinB1-Fc solution for 45 min. Afterwards the stamps were thoroughly rinsed with PBS and Milli-Q water and air dried. Inked stamps were brought into conformal contact with previously poly-L-lysine coated surfaces for 10 min. Flat stamps were carefully removed and conjugated ephrinB1-Fc or Human IgG_1 Fc were transferred to the surface. After printing, surfaces were rinsed with PBS and Milli-Q water. Stimulations with the soluble ligand were carried out as commonly used in the field. A DMEM solution of 0.4μM of either ephrinB1 or Fc were incubated with Recombinant Human IgG_1 Fc (R&D Systems Inc.) at a 1:5 mass ratio, for 30 minutes under constant shaking. After warming up at 37°C, 1 ml of the solution was added to the culture plate to reach a final 0.2μM concentration.

For every experiment, approximately 10^6 cells where freshly harvested from a culture plate and gently resuspended in DMEM without phenol red for immediate use. The cell suspension was then transferred into the functionalized plates containing either the micro-printed or soluble ligand, and spun down using a plate centrifuge at 1000rpm for 1 minute. When using the micro-printed plates, the clock was set to zero at the end of the centrifugation process. The samples were then quickly taken to the microscope for observation.

FCS and RICS measurements of EphB2 mobility

HEK293T cells were seeded into LabTek glass bottom chamber slides (Nalgene) and transiently co-transfected with a paGFP tagged EphB2 and membrane localizing mCherry (mem-mCherry) (Fig. S3). 24h following transfection cells were imaged using a Zeiss LSM 780 laser scanning confocal microscope and avalanche photodiodes of the Confocor 3 (Zeiss, Jena). A water ×63/1.4 NA objective (Zeiss, Jena) was used for imaging, photoactivation, paFCS and RICS. The paGFP was photoactivated with the 405 nm laser line for FCS and RICS acquisition following previously described protocols (46). FCS and RICS data were acquired using the ZEN Software FCS and RICS modules (Zeiss, Jena), respectively. For FCS acquisition, a point was selected along the membrane identified with the mem-mCherry marker and acquired for 25s with 4 repetitions, and analyzed through previously established paFCS protocols probing for anomalous and free diffusion (46). RICS data was performed by acquiring 100 consecutive frames with a 50 nm pixel size and pixel dwell time of 25 μs. Region-of-Interest analysis was performed by selecting small

regions along the membrane, and was fit to a single species. For both analyses the laser waist (ω_r) was calibrated as previously outlined (47).

Image acquisition

The diffusion rate of EphB2 was measured using standard single point FCS and Raster Image Correlation Spectroscopy (RICS) (47) and analyzed using ZEN (Zeiss, Jena, DE) and SimFCS (www.lfd.uci.edu) obtaining a value of 0.25+/- 0.08 $\mu m^2/s$.

We acquired the time series for N&B analysis using a commercial STORM microscope system from Nikon Instruments (NSTORM) equipped with an EMCCD camera (Andor iXon3 897) set to frame transfer mode and a 1.4 NA 100x objective and a 1.5x lens tube for additional magnification. The microscope was used in TIRF mode to illuminate only the portion of the cell membrane in direct contact with the glass surface. Cells were illuminated with 561nm light at low laser intensity (3 W/cm^2 power density) for 200 frames with 500 ms exposure time (1min 40sec total acquisition time). Every time-point acquisition was initiated 2 to 3 minutes after the termination of the previous one. Acquisition of every time point Exposure time was chosen so it fell in the linear range of the autocorrelation curve shown in Fig. S3. Waiting time between time points was 2.5 minutes. Camera calibration for N&B with dark was performed using SimFCS (www.lfd.uci.edu). Further processing was done with custom Matlab scripts (will be published elsewhere).

Cells used for monomer calibration were seeded for 24h on PLL. The value of Brightness retrieved for monomer was B(monomer)=1.17 with sigma = 0.08. The acquired data was detrended using boxcar filtering on each pixel. This detrending mode has been demonstrated to maintain fluctuations while improving the performance of N&B (43, 44). The values of aggregates were calculated as percentages from the Brightness histogram using the formula B(nmer) = 1+(n*(B(monomer)-1)) with variance measured from monomer calibration.

Cells undergoing apoptosis and out of the TIRF evanescent wave focal plane were excluded from analysis.

Enhanced Number and Brightness analysis

In this work we use the Number and Brightness (N&B) method (20) to measure the average number of molecules and brightness in each pixel of the fluorescent images acquired. N&B is a powerful tool that distinguishes pixels with different aggregation states by determining the mean intensity and variance of their relative fluorescence intensity fluctuations. The method has been successfully applied in both confocal (20, 22, 23) and EMCCD based systems (23) for measuring aggregation of proteins (22, 30, 48). In its most general form, the apparent Brightness, which represents the molecular aggregation level, is

calculated as the ratio of variance to average intensity while the apparent molecular Number is the ratio of total intensity over Brightness:

$$B = \frac{\sigma^2}{\langle k \rangle}$$

$$N = \frac{\langle k \rangle^2}{\sigma^2}$$

Step 1. Oligomerization enhancement. We acquire multiple time point datasets of the same specimen over approximately 60 minutes and apply N&B analysis to map the EphB2 receptor aggregation over time. However, the original N&B method has been used to give an averaged Brightness and Number for a given pixel over one contiguous dataset of F images acquired over one specific time range (tn) of the aggregation. In this work, we enhanced the resolution capability of the method by calculating within each pixel the distribution of aggregates and its dynamic over multiple time points (t1,t2,..tn). We name this the enhanced Number and Brightness (eN&B).

The enhancement is accomplished by analyzing the dataset with a circularly sliding window through the number F=200 of frames acquired in each time point. The analysis window was chosen to have length w=100 to provide a stack size with statistical confidence, 5 times larger than the minimum number suggested in the original N&B paper [17]. The analysis window was applied on the dataset with the same principle of circular buffers, in which we sub-sample the overall frames to build statistical distribution. The approach we chose uses the same size for this circular sliding window therefore ensuring same statistical weight to each frame and each Brightness calculated. Hence for each pixel (i,j) we obtain an array of F values of Brightness B. Each Brightness arise from a sliding window defined as follow:

$$B_s = \begin{cases} \left.\frac{.\sigma^2}{\langle k \rangle}\right|_n^{n+w} & if\ n < F - w \\ \left.\frac{.\sigma^2}{\langle k \rangle}\right|_n^{F} + \left.\frac{.\sigma^2}{\langle k \rangle}\right|_1^{w-(F-n)} & if\ n > F - w \end{cases}$$

where s goes from 1 to F. $\left.\frac{.\sigma^2}{\langle k \rangle}\right|_n^{n+w}$ is the B arising from the window of length w starting from position n and ending in n+w while $\left.\frac{.\sigma^2}{\langle k \rangle}\right|_n^{F} + \left.\frac{.\sigma^2}{\langle k \rangle}\right|_1^{w-(F-n)}$ joins frames from position n to last frame F and from position 1 until reaching the number w

Similarly we obtain corresponding F values of apparent Number N.

$$N_s = \begin{cases} \left.\frac{\langle k \rangle^2}{\sigma^2}\right|_n^{n+w} & if\ n < F - w \\ \left.\frac{\langle k \rangle^2}{\sigma^2}\right|_n^{F} + \left.\frac{\langle k \rangle^2}{\sigma^2}\right|_1^{w-(F-n)} & if\ n > F - w \end{cases}$$

As the sliding window maintains the time structure, this method can be considered as consecutive N&B measurement with time delay equals to the frame rate. After repeating the analysis for T time points we obtain a 5 dimensional hypercube of information with x, y pixel position, distribution of apparent Number and apparent Brightness in each pixel, and time.

Step 2. Time enhancement. The aggregation dynamics of EphB2 are captured, and analyzed using eN&B over multiple time point datasets to build a time evolution of the oligomerization. We enhanced the time resolution of eN&B by applying a set of detrending algorithms, which has been developed and optimized for reducing the effect of photobleaching on N&B while preserving the fluctuations(43, 44).

Oligomer calculation

The values of aggregates were calculated from the brightness distributions using the formula B(i-mer) = 1+(i*(B(monomer)-1)) with the spread measured from monomer calibration.

I-mer plots calculation

The time-evolution of oligomers is represented on i-mer plots. The parameters A_i and R_0 of experimental data were directly extracted from eN&B analysis. A_i is the relative concentration of each oligomer of size i (i-mer) which results from the sum of the concentrations of oligomers with same size, for all pixels in a cell. The relative concentration of every i-mer is described in the previous section. R_0 is the total concentration of receptors at the initial time-point calculated as $R_0 = R(t_0) + \sum_{i=2}^{N} i \cdot A_i\ (t_0)$. The theoretical calculation of A_i and R_0 is described the equation (19) from section 3 of the SI Text.

Automatic tracking of EphB2 clusters

Tracking was performed on one the dataset from cells stimulated with micro-printed ligand using Bitplane Imaris software and targeting the top 10% brightest aggregates. The sequence of 200 frames (100 sec) ensures statistical confidence with over 120.000 tracks performed.

Statistics

Welch's t test was calculated using MATLAB. P values for Figs. 2b and 4b $P_{Sol}= 4.11*10^{-6}$, $P_{mp}= 1.78*10^{-11}$. Combining all samples, with both soluble and micro-printed ligand presentation, negative controls and mutant cell lines, we analyzed 312 cells distributed over 36 experiments. The results of the analysis were robust and reproducible across experiments (see Fig. S4).

Confocal videos

3D confocal videos of large clusters condensation (movies S5-7) were acquired using ZEISS LSM 5 Exciter confocal microscope and rendered using Bitplane Imaris.

Data Availability

All data supporting the findings of this study are available from the corresponding authors on request.

Code Availability

All custom scripts are available from the corresponding authors on request.

Dynamical model: Polymerization-Condensation model for the aggregate kinetics during EphB2 clustering process

This document presents a phenomenological and kinematic model for the formation of Eph-receptor clusters on cellular membranes, based on polymerization models developed by for protein aggregation in solutions [5, 8, 3]. Important modifications were done in order to account for the particulars of live-cell processes and the imaging techniques described before. Model self-consistency, calibrations with experimental data and studies on the model sensitivity to the parameters are presented in this supplementary material.

1 Nomenclature

χ := ratio between observable and total cell membrane surface [-]
H := concentration of unobservable monomer [mol m^{-2}]
R := concentration of observable (monomer) [mol m^{-2}]
L := ligand concentration [mol m^{-2}] / [mol m^{-3}]
C := ligand-receptor complex (monomeric) concentration [mol m^{-2}]
A_i := concentration of the aggregate of size i, $i-$mer [mol m^{-2}]
k_n := rate coefficient in $R + C \rightarrow A_2$ [mol^{-1} m^2 s^{-1}]
k_{hg} := rate coefficient in $A_i + H \rightarrow A_{i+1}$ [mol^{-1} m^2 s^{-1}]
k_{rg} := rate coefficient in $A_i + R \rightarrow A_{i+1}$ [mol^{-1} m^2 s^{-1}]
k_c := rate coefficient in $A_i + A_j \rightarrow A_{i+j}$ [mol^{-1} m^2 s^{-1}]
R_0 := initial monomer concentration [mol / m^2]
h := dimensionless monomer concentration at membrane (H/R_0) [-]
r := dimensionless monomer concentration in cytosol (R/R_0) [-]
a_i := dimensionless $i-$aggregate concentration (A_i/R_0) [-]
k'_n := normalized rate coefficient $k_n R_0$ [s^{-1}]
k'_{hg} := normalized rate coefficient $k_{hg} R_0$ [s^{-1}]
k'_{rg} := normalized rate coefficient $k_{rg} R_0$ [s^{-1}]
k'_c := normalized rate coefficient $k_c R_0$ [s^{-1}]
t := time [s]
t_n := $1/k'_n$, nucleation characteristic time [s]
t_{hg} := $1/(k'_{mg}\chi)$ chain polymerization by unobservable monomer characteristic time [s]
t_{rg} := $1/k'_{rg}$ chain polymerization by addition of membrane receptor characteristic time [s]
t_c := $1/k'_c$ condensation characteristic time [s]
λ_0 := $\sum A_j/R_0 = \sum a_j$. 0-th order moment of the aggregate size distribution [-]
λ_1 := 1-st order moment of the aggregate size distribution [-]
λ_2 := 2-nd order moment of the aggregate size distribution [-]
μ := mean aggregate size [-]
σ^2_μ := variance in the aggregate size [-]
B := Brightness [Au]
N := Number [Au]
$\tilde{a}_i$:= dimensionless observable $i-$aggregate concentration from N and B histograms [-]

2 Assumptions, model derivation and equations

The enhanced Number and Brightness (eN&B) technique using TIRF microscopy quantifies the time-evolution of the different aggregates on the cell membrane on the bottom part of the cell, in contact with the plate or equivalently, in the imaged focal plane. Consequently, not all the cell is observed but only the focal plane. In the derivation of a kinetic model that can be fitted and compared to the experimental data, a division is required between the monomeric Eph receptors located in the focal plane, and thus is observed and measured by eN&B, and the receptors out of the focal plane and consequently unobservable or "hidden" to the experiment. Due to diffusion within the membrane, the unobservable receptor plays a fundamental role on the kinetics also in the focal plane.

Two different methodologies for the ligand presentation are considered in the present paper. In the first one, the ephrin ligand is microprinted homogeneously in the plate. Consequently, the formation of ligand-receptor complexes and initiation of the polymerization process can only happen in the membrane portion in contact with the plate, which is the area accessible to imaging and quantification by the eN&B technique. The second presentation method introduces the ligand in solution, therefore the nucleation process is distributed over the entire cell membrane. In this second method, nucleation is more heterogeneous in the observed part of the cell membrane than in the microprinted case, but conversely the observed part of the membrane is representative of the entire membrane.

The kinetic model will first be developed considering microprinted ligand; however, the same equations model the process with soluble ligand, though the interpretation of one parameter differs.

2.1 Polymerization-condensation model

Before the clustering process is initiated, only free monomer is assumed to be present in the membrane, with an homogeneous concentration. It is also assumed that the total Eph receptor number count in the membrane does not change noticeably along the characteristic times of the clustering process due to balanced synthesis and degradation rates, but only due to internalization of oligomers when they reach a certain size.

In the present model, nucleation occurs in two steps that, however, do not correspond exactly to those in the folded/unfolded nucleation of the Lumry-Eyring model [4]. In the first step, a suitable Eph receptor monomer (assumed to be in the adequate unfolded state) binds a ephrin ligand to form a complex,

$$R + L \rightarrow C. \tag{1}$$

This union can be reversible or irreversible, and is governed by the ligand and receptor concentrations (L and R) among other parameters, like receptor-ligand affinity or their respective diffusitivity. More importantly, this formation of an initial ligand-receptor complex accounts for the initial activation that triggers the phosphorylation process. Considering the microprinted ligand, Eph - ephrin complexes can only be formed on the plate, and then only the observed monomer R concentration is relevant. The unobserved monomer H, out of the plate, is not presented to the ligand.

In the second step, a complex (i.e. a phosphorylated receptor) binds to a second free monomeric Eph receptor, which hereafter will be treated as an Eph dimer:

$$C + R \rightarrow A_2. \tag{2}$$

Here, A_2 denotes the concentration of the dimer. This reaction is assumed to be irreversible. A constant k_n defines the total nucleation reaction rate, that accounts for the combined rate of monomer diffusion in membrane, ligand concentration, rate of collision between receptor and ligand and probability of complex and free monomer to aggregate after collision. Whether the second Eph receptor (R) was previously bound to a ligand before its binding to the first complex

(producing the basic Eph-ephrin heterotetramer) is irrelevant to the present kinetic model, which assumes that the phosphorylation of the first complex triggers the cluster formation. Therefore, no distinction will be done in what follows between monomeric Eph receptor or Eph-Ephrin complexes. Additionally, it is assumed that the characteristic times for the nuclei formation are short enough to neglect migration of the unobserved monomer H from other membrane regions to the plate. This assumption is confirmed latter by fitting model parameters to eN&B data, which shows that nucleation times are negligible against times for cluster formation, in which monomer migration becomes relevant.

Once a nucleus A_2 is formed, the cluster formation is modeled as a polymerization process, which is subsequently independent on the ligand concentration and occurs simultaneously through the following two phenomena:

(i) Addition of monomer receptor to existing oligomer to form a larger aggregate

$$A_i + R \to A_{i+1} \quad \text{and} \quad A_i + H \to A_{i+1} \tag{3}$$

(ii) Binding of existing oligomers to originate a larger aggregate

$$A_i + A_j \to A_{i+j}. \tag{4}$$

The two kind of reactions are assumed to be irreversible. The first kind of reaction (i) is termed chain polymerization in the literature [6, 1, 8], and modeled by a reaction rate coefficient k_g which is independent of the size of the aggregate assembled: these reactions are dominated by the diffusion of the monomer, either in the observable membrane (R) or in the unobservable part (H), and the aggregate size has a negligible effect.

The second kind of reaction (ii) is termed condensation, involves exclusively oligomeric aggregates in the membrane, and is governed here by a rate coefficient k_c. In general, this is a rough approximation as the reactions' rate coefficients are likely to depend on the size of the aggregates. Polymerization models in literature [5, 8, 3] consider a set of constants k_{ij} for the binding of aggregates of sizes i and j, resulting in the so-called aggregation kernel. Two different aggregation kernels are tested in this work. The first one is a constant one, i.e.

$$k_{ij} = 1 \quad \text{for all} \quad i, j \geq 2. \tag{5}$$

The second one is based on the diffusion-limited Smoluchowski model along with Stokes-Einstein equation for diffusion coefficients [3]:

$$k_{ij} = \frac{1}{4}\left(\frac{1}{i} + \frac{1}{j}\right)(i + j). \tag{6}$$

Controversy exists in the literature regarding the use of the Stokes-Einstein equation for diffusion on protein membranes. Stokes-Einstein equation, which states that diffusion is proportional to r^{-1} (where r is the characteristic size of the molecule), was originally derived for diffusion on three-dimensional media. Saffman and Delbrück [7] proposed a model for diffusion on membranes that scales as $\log(r^{-1})$. However, Gambin *et al.* [2] compared diffusions measured in a variety of bilayer membranes and concluded that the measured diffusion scales closely to r^{-1}, that is, according to Stokes-Einstein equation. However, it should be noted that an aggregation kernel based on the diffusion-limited Smoluchowski model with Saffman-Delbrück diffusion would produce results that lay between those produced by models (5) and (6). As will be shown later, both models deliver quantitatively similar results, and so would an aggregation kernel based on Saffman-Delbrück model.

The aggregate size is limited for two reasons. The first one is related to the progressive reduction of the associated diffusion as the aggregate grows, which translates in $k_{i,j} \to 0$ when $i \to \infty$ for model (6). The second one accounts for the action of endocytosis which removes aggregates from the membrane once they reach a threshold size, arbitrarily set up at aggregate N. The effect of this truncation is further discussed later in this supplementary material.

2.2 Kinetic equations for nucleation-polymerization

The parameter χ defines the fraction of the cell membrane exposed to ligand. For microprinted-ligand presentation, as all ligand is contained in the focal plane, χ also approximates the fraction of the cell membrane which is observable by the eN&B technique.

As stated before, the monomeric receptor is considered separately for the observable (or realizable) part of the cell membrane and for the unobservable one, and their respective concentrations are denoted by R and H respectively. Before initiation of nucleation-polymerization process, the monomer concentration is assumed to be homogeneous, $R(t=0) = H(t=0) = R_0$. The chain-polymerization reaction rates for observable and unobservable monomer (k_{rg} and k_{hg}) could, in principle, be considered as different. This accounts for the relatively different diffusion times from within the observed part of the membrane and the unobservable one. However, factors other than diffusion affect the reaction rate and, as will be shown later, both rates can be assumed to be equal. Finally, it is also assumed that the import of monomer from the unexposed regions to the ones in which clustering has been initiated is immediately consumed by polymer growth and does not add to the observable monomer. Consequently, depletion of the monomer observed by the eN&B technique occurs, for the cases with microprinted ligand, in times shorter than those typical of the clustering process, during which monomer is still available but cannot be observed with the present technique.

The system of governing equations in dimensional form is

$$\frac{\mathrm{d}H}{\mathrm{d}t} = -k_{hg}\chi H\left(\sum_{j=2}^{N-1} A_j\right), \tag{7}$$

$$\frac{\mathrm{d}R}{\mathrm{d}t} = -2k_N R^2 - k_{rg}R\left(\sum_{j=2}^{N-1} A_j\right), \tag{8}$$

$$\frac{\mathrm{d}A_2}{\mathrm{d}t} = k_N R^2 - (k_{hg}H + k_{rg}R)A_2 - \left(\sum_{j=2}^{N-1} k_{2,j}A_2A_j\right) - k_{2,2}A_2^2, \tag{9}$$

$$\frac{\mathrm{d}A_i}{\mathrm{d}t} = (k_{hg}H + k_{rg}R)(A_{i-1} - A_i) + \left(\sum_{j=2}^{i/2} k_{j,i-j}A_jA_{i-j}\right) - \left(\sum_{j=2}^{N-1} k_{i,j}A_j\right)A_i - k_{i,i}A_i^2, \quad i = 3,\ldots,N. \tag{10}$$

When index i in the last equation is odd, the right-most summation ends at $(i-1)/2$ instead of $i/2$. This upper limit in the summation avoids counting the combinations twice.

A scaled form is adopted now, by scaling the concentrations with the total receptor concentration at initial time, R_0, leading to $h := H(t)/R_0$, $r := R(t)/R_0$ and $a_i := A_i(t)/R_0$. This normalized form of the equations is convenient as it eliminates the dependence of the constants on the initial monomer concentration, thus making it possible to compare parameters for different cells. The normalized rate coefficients are defined as $k'_n = k_nR_0 = 1/t_n$, $k'_{hg} = k_{hg}R_0 = 1/\chi t_{hg}$, $k'_{rg} = k_{rg}R_0 = 1/t_{rg}$ and $k'_c = k_cR_0 = 1/t_c$, where t_n, t_{hg}, t_{rg} and t_c are characteristic times for the nucleation, chain polymerization and condensation phases.

The kinetic equations for the evolution of dimensionless variables in dimensional time t are:

$$\frac{\mathrm{d}h}{\mathrm{d}t} = -\chi h\left(\sum_{j=2}^{N-1} k'_{hg}a_j\right), \tag{11}$$

$$\frac{\mathrm{d}r}{\mathrm{d}t} = -2k'_n r^2 - k'_{rg}r\left(\sum_{j=2}^{N-1} a_j\right), \tag{12}$$

$$\frac{\mathrm{d}a_2}{\mathrm{d}t} = k'_n r^2 - (k'_{hg} h + k'_{rg} r) a_2 - \left(\sum_{j=2}^{N-1} k'_{2,j} a_j \right) a_2 - k'_{2,2} a_2^2, \tag{13}$$

$$\frac{\mathrm{d}a_i}{\mathrm{d}t} = (k'_{hg} h + k'_{rg} r)(a_{i-1} - a_i) + \left(\sum_{j=2}^{i/2} k'_{j,i-j} a_j a_{i-j} \right) - \left(\sum_{j=2}^{N-1} k_{i,j} a_j \right) a_i - k'_{i,i} a_i^2, i = 3, \ldots, N. \tag{14}$$

2.3 Considerations for soluble-ligand presentation

The kinetic model derived for microprinted ligand can also be applied to soluble ligand. The clustering process in this case occurs equally over the entire cell membrane and the part of the cell observed by the eN&B technique is representative of the rest of the cell. Numerical values for χ and H consequently differ remarkably from those for microprinted ligand. Limit values $\chi = 1$ and $H = 0$ are not imposed, as they account for second-order effects like newly-synthesized monomer, that were negligible in the kinetics of microprinted ligand.

2.4 Moments of the aggregate number distributions

Let λ_0, λ_1 and λ_2 denote the 0-th, 1-st and 2-nd order moments of the aggregate size distributions:

$$\lambda_0 = \sum_{i=2}^{\infty} a_i, \quad \lambda_1 = \sum_{i=2}^{\infty} i a_i, \quad \text{and} \quad \lambda_2 = \sum_{i=2}^{\infty} i^2 a_i. \tag{15}$$

The three moments are functions of time. In the case that $\chi = 1$, then $h = 0$ and $\lambda_1 = 1 - r$, implying conservation of the receptor number count.

2.5 Mean and variance of the aggregate number

The relative importance of the two mechanisms at play during the clustering process, namely chain-polymerization and condensation, can be illustrated by monitoring the mean aggregate number μ and its covariance σ_μ^2, defined as

$$\mu = \frac{\sum_{i=1}^{N} i a_i}{\sum_{i=1}^{N} a_i} = \frac{\lambda_1}{\lambda_0}, \tag{16}$$

and

$$\sigma_\mu^2 = \frac{\sum_{i=1}^{N} i^2 a_i}{\sum_{i=1}^{N} a_i} - \mu^2 = \frac{\lambda_2}{\lambda_0} - \left(\frac{\lambda_1}{\lambda_0} \right)^2. \tag{17}$$

In a clustering process with no condensation, and under the hypothesis of the present model, variance equals the mean aggregate size, as the dispersion of the concentration distribution remains constant. On the other hand, for processes dominated by condensation the variance grows much faster than the mean aggregate number, and $\sigma_\mu^2 \gg \mu$ until effects related to a maximum aggregate size (100 in the model) come into play.

Alternative quantifications of the competence between the chain-polymerization and the condensation can be found in the literature. The most extended one monitors the polidispersity [3], which is related to the mean and variance by

$$P = 1 + \frac{\sigma^2}{\mu_\sigma^2}. \tag{18}$$

The two separated magnitudes are considered here, as they provide additional useful information.

2.6 Relation between clustering process and tyrosine kinase activation

The current model for the Eph receptor activation states that phosphorylation of relevant tyrosine residues on each receptor is mediated by dimerization and the binding of free monomers to pre-phosphorylated receptors [9]. Consequently, the temporal evolution of the tyrosyne kinase activity is assumed to be proportional to the accumulated number-weight of the aggregates (equivalent to the first-order momentum) λ_1.

3 Fitting the model parameters with enhanced Number and Brightness data

The experiments acquire images of the cell membrane in contact with the plate, the rest of the cell remaining unobserved. The eN&B technique delivers distributions of apparent concentrations per pixel and time instant which gives a statistically representative evolution of the aggregate concentrations over time, $\tilde{A}_i(t)$ ($\tilde{A}_1 = \tilde{R}$, the observed apparent concentration of monomer).

During the initial 10-15 minutes the cell settles down in the plate. In this period the nucleation process is dominant. Afterwards, for microprinted ligand, the receptor aggregation process turns into a regular pattern of polymerization by addition of monomer, in which the concentrations of successive oligomers grow, saturate and decay in a very ordered manner, typical of Type II kinetics described by [1]. Condensation is also present and becomes revealed by moments analysis. The condensation is better visualized by monitoring the evolution of the mean polymer size μ and its standard deviation σ_μ: while in pure chain-polymerization both grow with the same rate, in condensation-dominated processes the aggregate's dispersion increase, and the standard deviation grows much faster. Using the soluble ligand presentation as a reference (where the effect of the unobservable monomer is minimized), the duration of chain polymerization approximately stops with the depletion of observable monomer.

The model constants are determined by fitting with the experimental data only in the intermediate temporal region. Initial concentrations $\tilde{R}$ and $\tilde{A}_i$, $i = 1, \ldots, N$ are taken typically at the third measurement time ($t \sim 20$ mins) and used to estimate the concentration of monomer before activation: as stated before, it is assumed that the Eph receptor number count does not change noticeably on the first 20-30 minutes of the experiment, so that

$$R_0 = \tilde{R}(t_0) + \sum_{i=2}^{N} i\tilde{A}_i(t_0). \tag{19}$$

Once R_0 is determined, the normalized concentrations $\tilde{r}(t)$, $\tilde{a}_i(t)$ are computed. The characteristic times $t_n, t_g = t_{hg} = t_{rg}$ and t_c are determined by a least squares minimization for $\mathrm{R}^2 - 1$, where R^2 is the coefficient of determination:

$$\mathrm{R}^2 := 1 - \frac{SSR}{SST} = 1 - \frac{\sum_{t=t_0}^{t_f} |\mathbf{a}(t) - \tilde{\mathbf{a}}(t)|^2}{\sum_{t=t_0}^{t_f} | < \tilde{\mathbf{a}} > -\tilde{\mathbf{a}}(t)|^2}, \tag{20}$$

where $\tilde{\mathbf{a}}$ is the vector $[r, a_2, a_3, \ldots, a_N]^T$ at each time instant obtained from eN&B, $\mathbf{a}$ is the solution of the kinetic model equations integrated from time $t = t_0$ to t_f, with initial condition $\tilde{\mathbf{a}}(t_0)$, and

$$< \tilde{\mathbf{a}} >= \frac{1}{t_f - t_0} \sum_{t=t_0}^{t_f} \tilde{\mathbf{a}}(t). \tag{21}$$

4 Model fitting, validations and results

Tables 1 to 4 show the best fitting parameters in the sense of reducing R^2 for some selected cases and χ values, for the two models of the aggregation kernel considered and for a series of cells with microprinted and soluble ligand. The range of experimental time instants used in the fitting for each case is also shown. The largest aggregate allowed is $N = 100$ for these fittings. Only small differences are observed between the fitted models for the constant aggregation kernel for condensation and the more complex one given by [3, 2], the former resulting in slightly better agreements with the experimental data.

Figures 1 and 2 compare the evolution of the normalized aggregate concentrations for two cases with microprinted ligand. The figures show the evolution of the concentration of representative aggregates between monomer and 40-mer, and the evolution of the mean and variance of the aggregate size. The best fitting parameters are used for each case, taken from the fitting tables.

Figures 3 and 4 show the analogous comparison for two cases with soluble ligand. In these cases the evolution of λ_1, assumed to be proportional to the tyrosine activation, is also shown as obtained from cell visualizations and the fitted model.

4.1 The influence of the aggregate truncation in the model results

To test the influence of the maximum aggregate size allowed in the model, it was computed using three different truncations, $N = 60$ and 40, for the microprinted and the soluble ligand cases. Figure 5 shows the percentage of the total receptor quantity,

$$\text{Apparent receptor} = r + \lambda_1, \tag{22}$$

and the relative accumulated number-weight of the aggregates (λ_1), as estimated by the model fitted with distributions obtained by eN&B. As exposed before, truncation in the model accounts for internalization of oligomers as they reach a threshold size. In the cases with microprinted ligand, the total quantity of receptor is nearly insensitive to the maximum aggregate size allowed. In the cases with soluble ligand the total quantity of receptor after 60 minutes is reduced between 28% -and- 2% if the maximum aggregate size is truncated, respectively, in the range of 40-mer to 100-mer. The difference is probably due to the formation of larger aggregates by the soluble ligand induction than by the microprinted one (as shown in Figures 2 and 3).

Bottom row on figure 5 shows the effect of aggregate truncation on λ_1, which is assumed to be proportional to the tyrosine kinase activation [9]. Again, cases with microprinted ligand are insensitive to the truncation, while qualitative differences become evident for the soluble ligand: For internalization of oligomer over 60-mer, the model predicts that the phosphorylation signal will reach a maximum value, then commence to decrease. The maximum signal amplitude, as well as the time for which it occurs, depends markedly on the maximum size of the oligomers allowed. As a consequence, fast condensation rates giving rise to large oligomers in short times can serve as a mechanism for dynamic range control.

These results show that the size of truncation (above 40-mer) has little impact in the aggregation dynamics for the microprinted case. In the soluble ligand case, the results suggest that truncating the maximum size below 100-mer may result in some loss of information only at later stages of the aggregation dynamics, but have an impact on tyrosine kinase signal.

4.2 Averaged evolution of oligomers

The eN&B data for several cells acquired at same time instants were averaged to produce representative evolutions for the different ligand concentrations. Table 5 shows the fitting parameters and coefficient of determination R^2 for two microscope positions for each plate. These data is also

interpolated to a refined time-grid, which enables us to average data from different experimental realizations for the two ligand concentration. The fitting parameters for the globally averaged data are shown in table 6.

Most interestingly, the maxima of the distributions provide the evolution of the dominant aggregate size, which together with the average and its standard deviation over time provide a broad picture of the active species in the oligomer population. Table 7 shows the corresponding values at minute 15 and 30, for ligand concentrations 0.2μM and 0.066μM. It should be expected that for lower ligand concentrations, the initial process of nuclei formation will be less efficient, which translates into the mean aggregates being smaller for a given time.

References

[1] J. M. Andrews and C. J. Roberts. A lumry-eyring nucleated polymerization model of protein aggregation kinetics: 1. aggregation with pre-equilibrated unfolding. *J. Phys. Chem. B*, 111:7897–7913, 2007.

[2] Y. Gambin, R. Lopez-Esparza, M. Reffay, E. Sierecki, N. S. Gov, M. Genest, R. S. Hodges, and W. Urbach. Lateral mobility of proteins in liquid membranes revisited. *Proc. Nat. Acad. Sci. USA*, 103(7):2098–2102, 2006.

[3] Y. Li and C. J. Roberts. A lumry-eyring nucleated polymerization (lenp) model of protein aggregation kinetics: 2. competing growth via condensation- and chain-polymerization. *J. Phys. Chem. B*, 113(19):7020–7032, 2009.

[4] R. Lumry and H. Eyring. Conformation changes of proteins. *J. Phys. Chem.*, 58:110–120, 1954.

[5] M. M. Pallitto and R. M. Murphy. A mathematical model of the kinetics of β-amyloid fibril growth from the denatured state. *Biophysical Journal*, 81:1805–1822, 2001.

[6] C. J. Roberts. Kinetics of irreversible protein aggregation: Analysis of extended lumry-eyring models and implications for predicting protein shelf life. *J. Phys. Chem. B*, 107:1194–1207, 2003.

[7] P. G. Saffman and M. Delbrück. Brownian motion in biological membranes. *Proc. Nat. Acad. Sci. USA*, 72(8):3111–3113, 1975.

[8] P. Sandkuhler, J. Sefcik, M. Lattuada, H. Wu, and M. Morbidelli. Modeling structure effects on aggregation kinetics in colloidal dispersions. *AIChE Journal*, 49(6):1542–1555, 2003.

[9] Andreas Schaupp, Ola Sabet, Irina Dudanova, Marion Ponserre, Philippe Bastiaens, and Rüdiger Klein. The composition of ephb2 clusters determines the strength in the cellular repulsion response. *The Journal of cell biology*, 204(3):409–422, 2014.

Table 1: Fitted coefficients, range of fitting and determination coefficient, using a constant aggregation kernel. Microprinted ligand (mp).

Case	range (frame$_0$:frame$_f$)	χ	t_n	t_g	t_c	R^2
mp Cell 1	3:11	0.01	0.05	2.25	30	0.9727
		0.03	0.05	2.25	30	0.9730
		0.05	0.05	2.25	30	0.9711
		0.1	0.05	2	30	0.9673
mp Cell 2	3:11	0.01	0.02	1.75	10	0.9474
		0.03	0.02	2	5	0.9467
		0.05	0.02	2	5	0.9458
		0.1	0.02	2	5	0.9415
mp Cell 3	3:11	0.01	0.05	2.5	20	0.9285
		0.03	0.1	2.5	20	0.9249
		0.05	0.1	2.5	20	0.9202
		0.1	0.05	2.75	10	0.9134
mp Cell 4	3:11	0.01	0.1	3	10	0.9746
		0.03	0.1	3	10	0.9743
		0.05	0.1	3	10	0.9736
		0.1	0.1	2.75	10	0.9720
mp Cell 5	3:11	0.01	0.02	2.25	10	0.9577
		0.03	0.02	2	10	0.9541
		0.05	0.02	2	10	0.9533
		0.1	0.02	2	10	0.9452
mp Cell 6	3:11	0.01	0.1	2.5	10	0.9646
		0.03	0.1	2.5	10	0.9626
		0.05	0.1	2.5	10	0.9596
		0.1	0.1	2.25	10	0.9544
mp Cell 7	3:11	0.01	0.1	3	11	0.9737
		0.03	0.1	3	11	0.9733
		0.05	0.1	2.75	11	0.9739
		0.1	0.1	2.75	11	0.9733
mp Cell 8	3:11	0.01	0.25	3.75	20	0.9555
		0.03	0.25	3.75	20	0.9542
		0.05	0.25	3.75	20	0.9526
		0.1	0.25	3.5	20	0.9486

Table 2: Fitted coefficients, range of fitting and determination coefficient, using a constant aggregation kernel. Soluble ligand (so).

Case	range (frame$_0$:frame$_f$)	χ	t_n	t_g	t_c	R^2
so Cell 1	3:10	0.01	0.02	4.5	7	0.9575
		0.03	0.02	4.5	7	0.9580
		0.05	0.02	4.5	7	0.9584
		0.1	0.02	4.25	7	0.9595
		0.25	0.02	4.25	7	0.9595
		0.5	0.02	2.5	7	0.9693
		0.75	0.02	2	7	0.9687
		1	0.02	1.75	7	0.9593
so Cell 2	3:10	0.01	0.25	3.75	12	0.9183
		0.05	0.25	3.75	12	0.9166
		0.1	0.25	3.75	11	0.9140
		0.25	0.25	3.5	11	0.9052
		0.5	0.25	3.25	9	0.8877
		0.75	0.25	3.25	8	0.8694
		1	0.25	3.25	7	0.8528
so Cell 3	3:10	0.01	0.5	5	15	0.7964
		0.1	0.5	5	15	0.8084
		0.25	0.5	5	20	0.8267
		0.5	0.5	5	20	0.8513
		0.75	0.5	5	20	0.8697
		1	0.5	5	20	0.8833
so Cell 4	3:10	0.01	0.005	2.25	20	0.9502
		0.05	0.005	2	20	0.9435
		0.1	0.005	2	15	0.9355
		0.25	0.005	1.75	15	0.8994
		0.5	0.005	1.75	11	0.8342
		0.75	0.005	2	9	0.7916
		1	0.005	2.25	9	0.7646

Table 3: Fitted coefficients, range of fitting and determination coefficient, using [3] aggregation kernel. Microprinted ligand (mp).

Case	range (frame$_0$:frame$_f$)	χ	t_n	t_g	t_c	R^2
mp Cell 1	3:11	0.01	0.05	2.25	30	0.9725
		0.03	0.05	2.25	30	0.9729
		0.05	0.05	2.25	30	0.9712
		0.1	0.05	2.00	30	0.9673
mp Cell 2	3:11	0.01	0.02	1.75	10	0.9345
		0.03	0.02	1.75	10	0.9483
		0.05	0.02	1.75	10	0.9464
		0.1	0.02	1.75	10	0.9348
mp Cell 3	3:11	0.01	0.1	2.5	20	0.9290
		0.03	0.1	2.5	20	0.9258
		0.05	0.1	2.5	20	0.9215
		0.1	0.1	2.25	20	0.9094
mp Cell 4	3:11	0.01	0.1	3	10	0.9748
		0.03	0.1	3	10	0.9749
		0.05	0.1	3	10	0.9745
		0.1	0.1	2.75	10	0.9722
mp Cell 5	3:11	0.01	0.02	2.25	10	0.9548
		0.03	0.02	2.25	10	0.9516
		0.05	0.02	2	10	0.9494
		0.1	0.02	2	10	0.9431
mp Cell 6	3:11	0.01	0.1	2.5	10	0.9646
		0.03	0.1	2.5	10	0.9626
		0.05	0.1	2.5	10	0.9596
		0.1	0.1	2.25	10	0.9544
mp Cell 7	3:11	0.01	0.1	3	11	0.9737
		0.03	0.1	3	11	0.9733
		0.05	0.1	2.75	11	0.9739
		0.1	0.1	2.75	11	0.9733
mp Cell 8	3:11	0.01	0.25	3.75	20	0.9555
		0.03	0.25	3.75	20	0.9542
		0.05	0.25	3.75	20	0.9526
		0.1	0.25	3.5	20	0.9486

Table 4: Fitted coefficients, range of fitting and determination coefficient, using [3] aggregation kernel. Soluble ligand (so).

Case	range (frame$_0$:frame$_f$)	χ	t_n	t_g	t_c	R^2
so Cell 1	3:10	0.01	0.02	4.75	8	0.9560
		0.05	0.02	4.5	8	0.9569
		0.1	0.02	4.25	8	0.9579
		0.25	0.02	3.75	8	0.9614
		0.5	0.02	2.75	8	0.9669
		0.75	0.02	2	8	0.9679
		1	0.02	1.75	7	0.9595
so Cell 2	3:10	0.01	0.25	4	12	0.9158
		0.05	0.25	3.75	12	0.9141
		0.1	0.25	3.75	12	0.9118
		0.25	0.25	3.5	12	0.9030
		0.5	0.25	3.25	10	0.8858
		0.75	0.25	3.25	9	0.8677
		1	0.25	3.25	8	0.8515
so Cell 3	3:10	0.01	0.5	5	20	0.7912
		0.05	0.5	5	20	0.7968
		0.1	0.5	5	20	0.8036
		0.25	0.5	5	20	0.8219
		0.5	0.5	5	20	0.8466
		0.75	0.5	5	20	0.8653
		1	0.5	5	20	0.8794
so Cell 4	3:10	0.01	0.005	2.25	20	0.9486
		0.05	0.005	2.25	20	0.9419
		0.1	0.005	2	20	0.9343
		0.25	0.005	1.75	15	0.8983
		0.5	0.005	1.75	12	0.8339
		0.75	0.005	2	10	0.7926
		1	0.005	2.5	9	0.7664

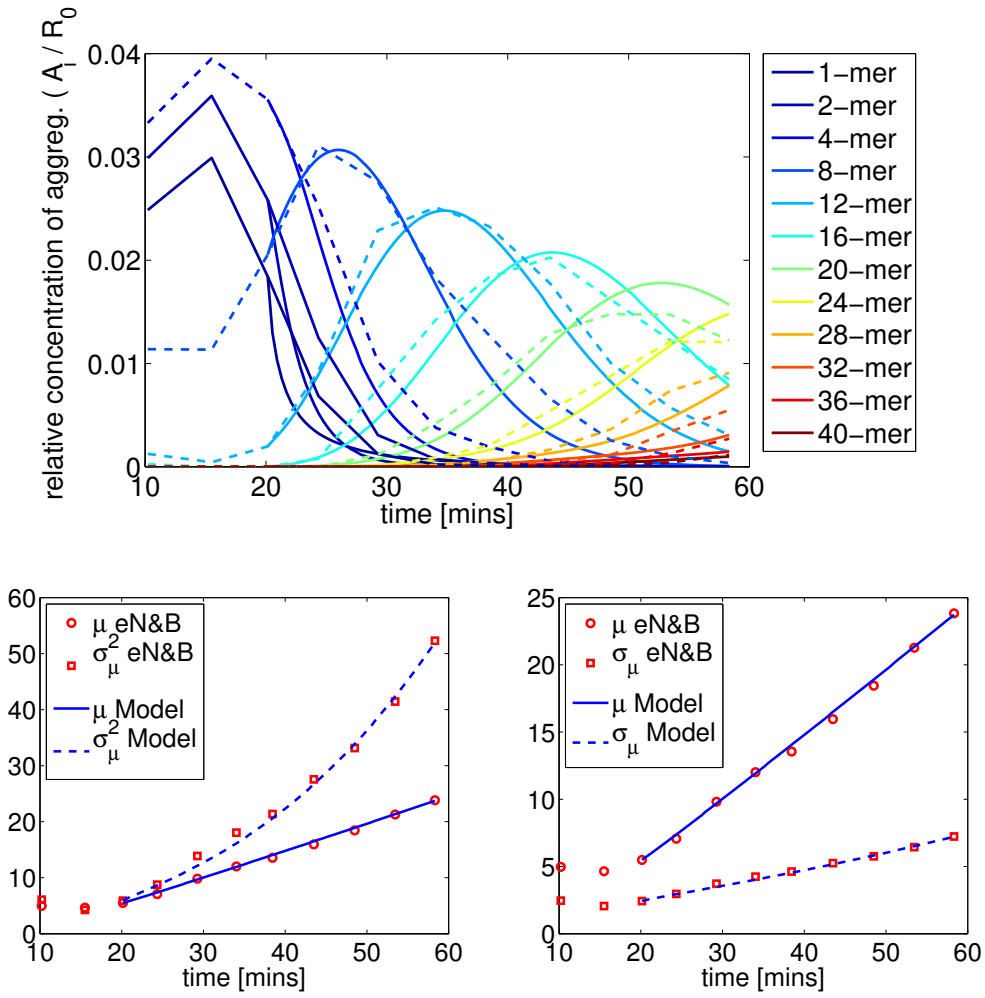

Figure 1: Time-evolution of the aggregate concentrations (top), and mean and variance or standard deviation of the aggregate size (bottom) from eN&B and model. Microprinted ligand Cell 1, $\chi = 0.01$, $t_n = 0.05$, $t_g = 2.25$, $t_c = 40$, for constant aggregation kernel. $R^2 = 0.9727$.

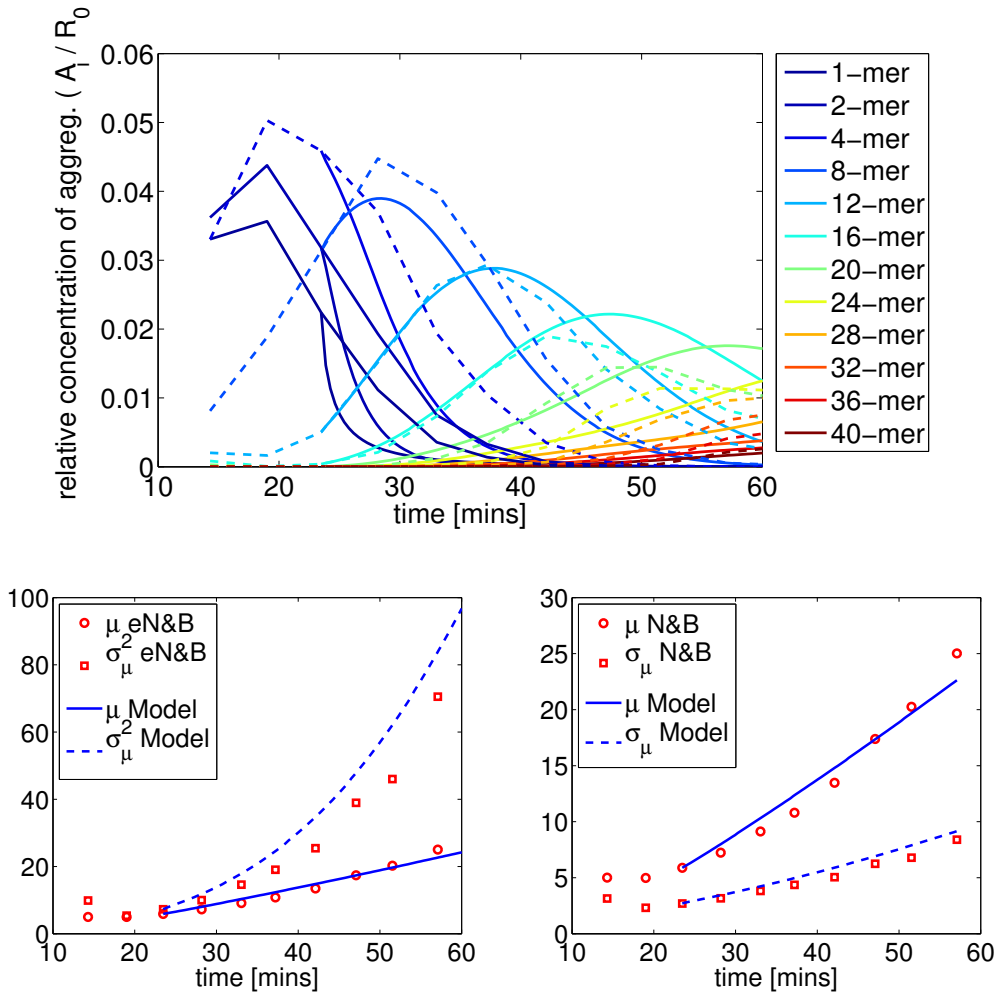

Figure 2: Time-evolution of the aggregate concentrations (top), and mean and variance or standard deviation of the aggregate size (bottom) from eN&B and model. Microprinted ligand Cell 3, $\chi = 0.01$, $t_n = 0.05$, $t_g = 2.5$, $t_c = 20$, for constant aggregation kernel. $R^2 = 0.9285$.

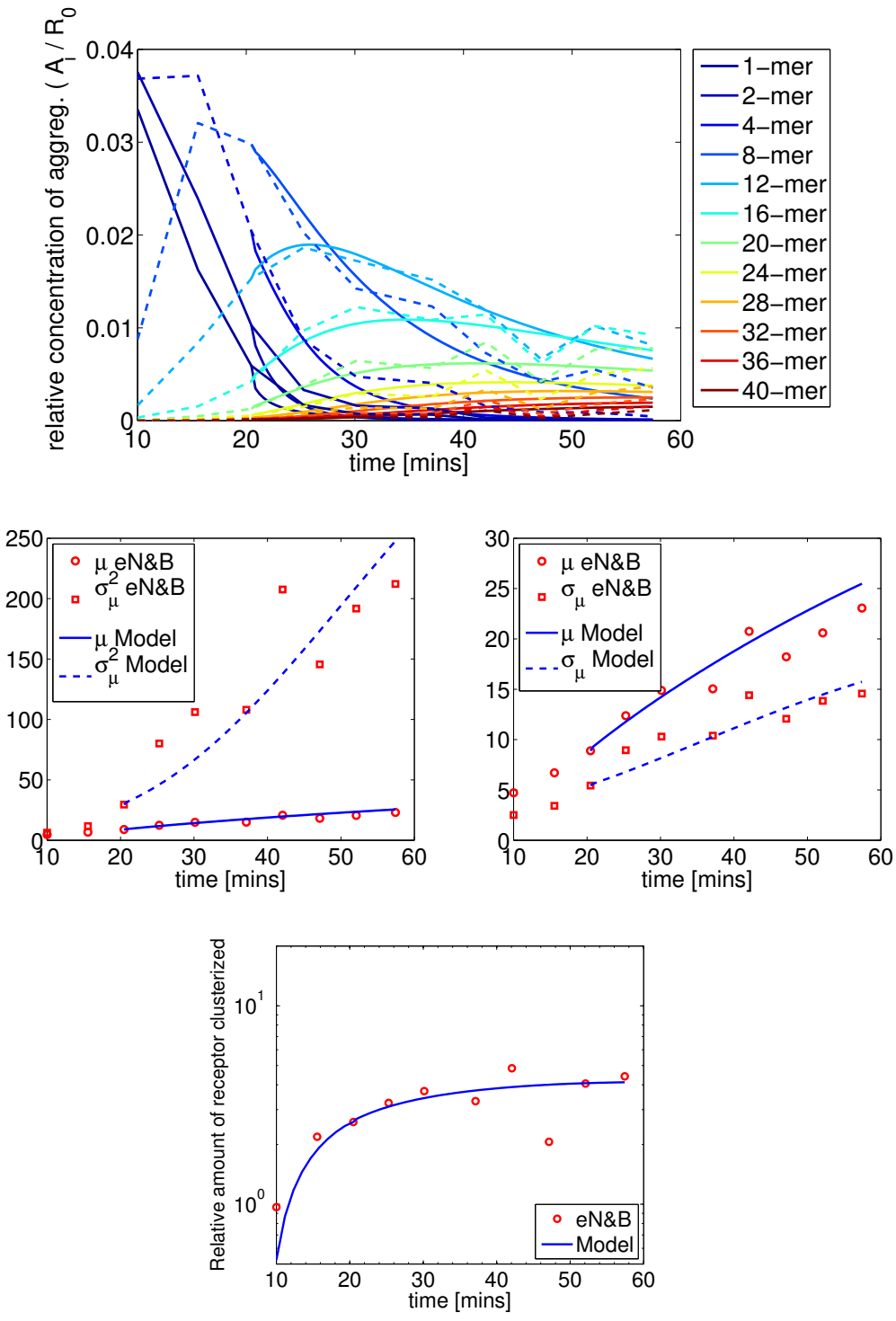

Figure 3: Time-evolution of the aggregate concentrations (top), mean and variance or standard deviation of the aggregate size (middle), and λ_1 (bottom), from eN&B and model. Soluble ligand Cell 1, $\chi = 0.5$, $t_n = 0.02$, $t_g = 2.5$, $t_c = 7$, for constant aggregation kernel. $R^2 = 0.9693$.

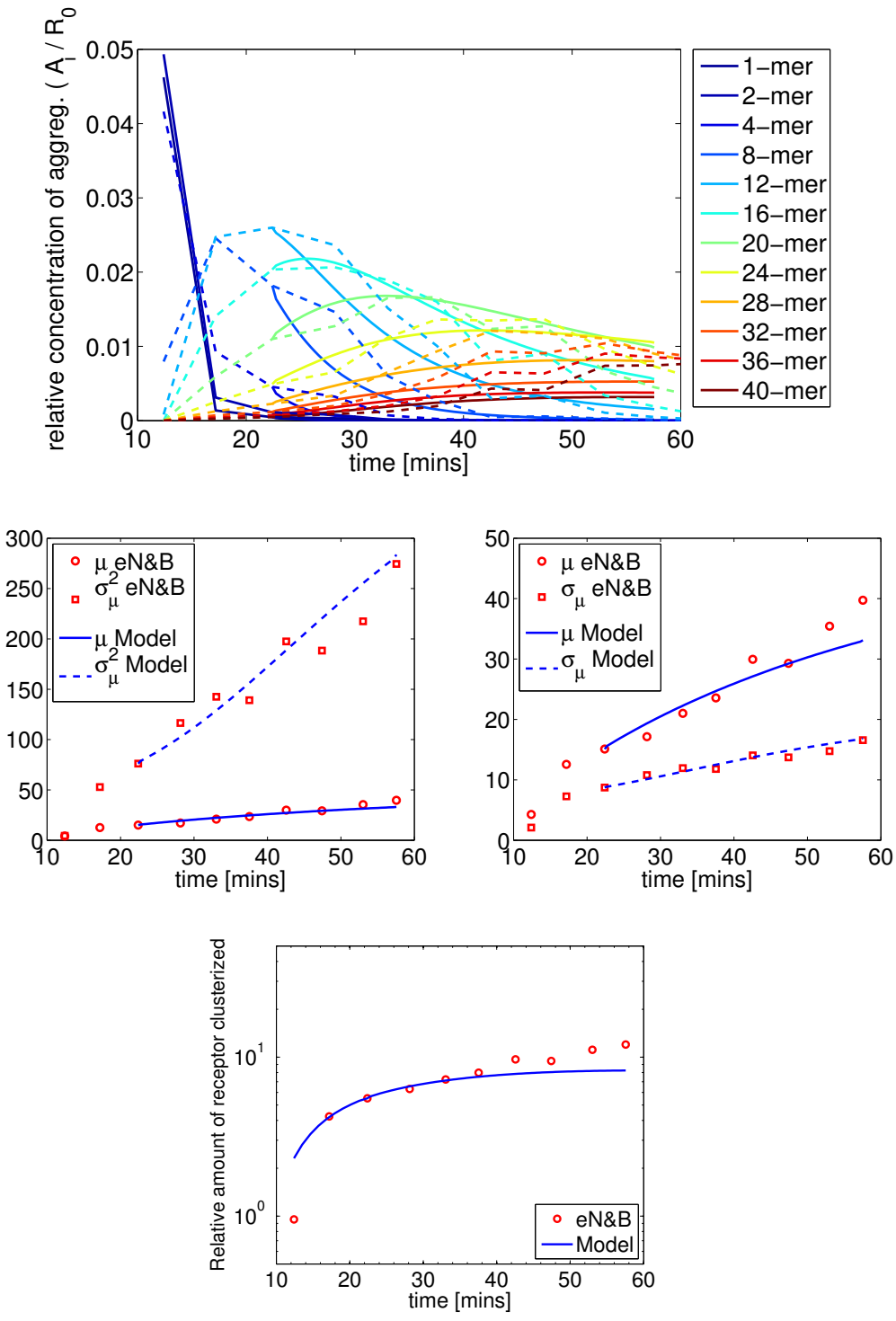

Figure 4: Time-evolution of the aggregate concentrations (top), mean and variance or standard deviation of the aggregate size (middle), and λ_1 (bottom), from eN&B and model. Soluble ligand Cell 4, $\chi = 0.25$, $t_n = 0.005$, $t_g = 1.75$, $t_c = 15$, for constant aggregation kernel. $R^2 = 0.8994$.

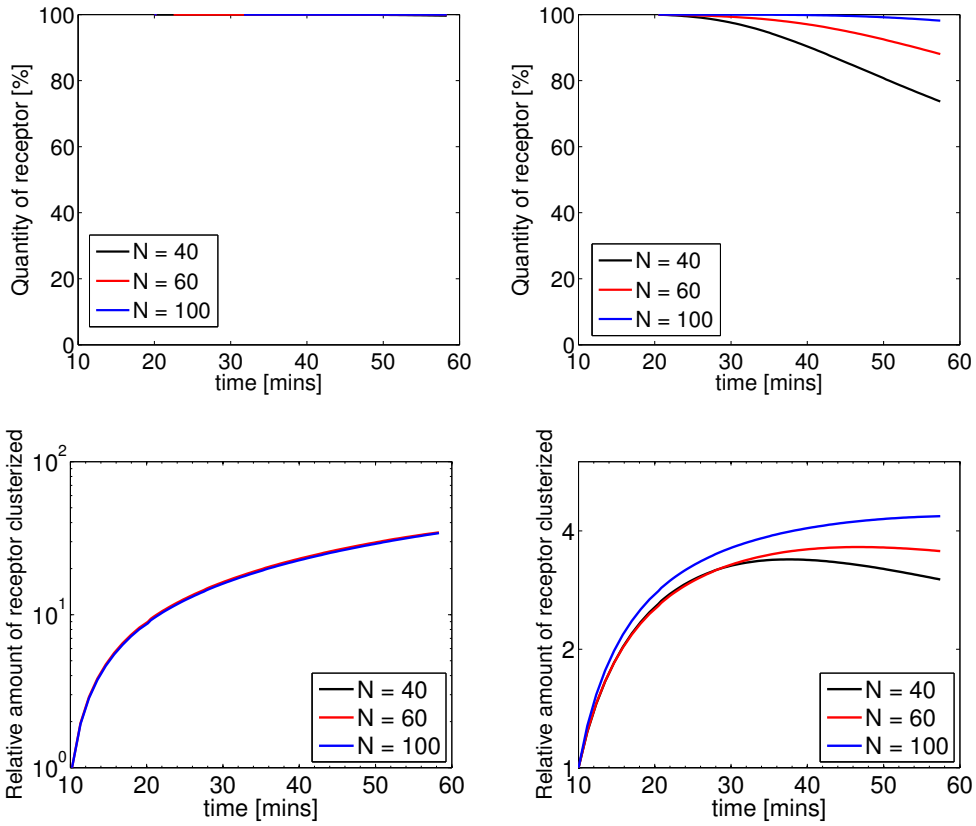

Figure 5: Evolution of the total receptor estimated by the model (top row) and relative number of clusterized receptor λ_1 (bottom row), for three maximum aggregate sizes: $N = 40, 60$ and 100. Left: Microprinted ligand Cell 1. Right: Soluble ligand Cell 1.

Table 5: Fitted coefficients, range of fitting and determination coefficient, using a constant aggregation kernel. Test with selection-averaged enhanced N&B data, for two different ligand concentrations.

Case	range frame$_0$:frame$_f$	χ	t_n	t_g	t_c	R^2
Plate 1, Position 1, 0.2μM	3:11	0.25	0.05	5	15	0.9604
		0.5	0.05	4.5	15	0.9613
		0.75	0.05	4	15	0.9613
		1	0.05	3.5	15	0.9600
Plate 1, Position 2, 0.2μM	3:11	0.25	0.02	5	12	0.9299
		0.5	0.02	4.5	12	0.9327
		0.75	0.02	3.75	12	0.9351
		1	0.02	3.25	12	0.9268
Plate 2, Position 1, 0.2μM	3:11	0.25	0.1	7	20	0.9749
		0.5	0.1	6.5	20	0.9731
		0.75	0.1	6	20	0.9706
		1	0.1	6	15	0.9671
Plate 2, Position 2, 0.2μM	3:11	0.25	0.1	7.5	20	0.9753
		0.5	0.1	6.5	20	0.9734
		0.75	0.1	6	20	0.9707
		1	0.1	5.5	20	0.9670
Plate 3, Position 1, 0.066μM	3:11	0.25	0.25	6	12	0.9108
		0.5	0.25	5.5	12	0.9073
		0.75	0.25	5	11	0.9033
		1	0.25	4.75	11	0.8991
Plate 3, Position 2, 0.066μM	3:11	0.25	0.25	8	10	0.9413
		0.5	0.5	8	10	0.9462
		0.75	0.5	8	10	0.9496
		1	0.5	8	10	0.9519
Plate 4, Position 1, 0.066μM	3:11	0.25	0.02	8	30	0.9400
		0.5	0.02	8	25	0.9387
		0.75	0.02	8	25	0.9362
		1	0.02	8	25	0.9325
Plate 4, Position 2, 0.066μM	3:11	0.25	0.25	8	40	0.9199
		0.5	0.25	8	40	0.9292
		0.75	0.25	8	40	0.9347
		1	0.25	8	40	0.9377

Table 6: Fitted coefficients, range of fitting and determination coefficient, using a constant aggregation kernel. Test with averaged enhanced N&B data, for two different ligand concentrations.

Case	χ	t_n	t_g	t_c	R^2
0.2μM	0.25	0.25	7.5	20	0.9757
	0.5	0.25	7	20	0.9747
	0.75	0.25	6.5	20	0.9732
	1	0.25	6	20	0.9713
0.066μM	0.25	0.5	8	30	0.9385
	0.5	0.5	8	30	0.9412
	0.75	0.5	8	25	0.9415
	1	0.5	8	20	0.9394

Table 7: Mean aggregate size (μ), most frequent aggregate size (max) and their respective standard deviations for $t = 15$ and 30 mins, for two different ligand concentrations. Test with globally-averaged enhanced N&B data.

	$t = 15$ mins				$t = 30$ mins			
Ligand concentration	μ	σ_μ	max	σ_{max}	μ	σ_μ	max	σ_{max}
0.2 μM	6.60	3.61	5.25	3.11	8.52	4.63	8.50	3.64
0.066 μM	4.91	2.68	4.10	0.93	7.01	4.05	7.19	2.36